Simulation of polymer chains in elongational flow. Steady-state properties and chain fracture

J. J. Lopez Cascales and J. Garcia de la Torre[a]
Departamento de Quimica Fisica, Universidad de Murcia, 30071 Murcia, Spain

The behavior of polymer chains in steady, uniaxial elongational flows is studied using the Brownian dynamics simulation technique. Two different types of chain models are considered. One is the bead-and-spring Rouse chain and the other is a chain with breakable connectors that obey a Morse potential. The dynamics of Rouse chains and Morse chains is simulated both without and with hydrodynamic interaction (HI) between chain elements. From the simulated trajectories, steady-state properties such as chain dimensions and elongational viscosities are calculated. When HI is accounted for by using the Rotne–Prager–Yamakawa tensor, the calculated dimensions and viscosities are appreciably lower than when it is neglected. Carrying out simulations with varying elongational rate, it is possible to observe stretching and finally the fracture of the polymer chains. The critical elongational rate, corresponding to infinite elongation in the case of Rouse chains, and the fracture of the Morse chains has been characterized as a function of chain length. When the short length of the simulated chains is accounted for adequately, we find that the elongational rate needed for fracture $\dot{\epsilon}_f$ scales with molecular weight M as $\dot{\epsilon}_f \propto M^{-2}$. This result, which had already been predicted rigorously without HI, holds in practice as well when hydrodynamic interaction is considered.

INTRODUCTION

When dilute polymer solutions are subjected to elongational flows with a sufficiently high stress rate, two salient phenomena show up.[1] One of them is the stretching of the otherwise coiled chains that is manifested as a sharp increase in some solution properties of the polymer such as chain dimensions and solution viscosity and birefringence. The other is the fracture of the polymer chains due to the mechanical stress produced by the viscous drag. These phenomena are quite complex, not only in regard to the nature of the interaction between the polymer and the flowing solvent,[2] but also because of the difficulties for the experimental realization of conditions that could be described theoretically with ease.

Notwithstanding such difficulties, theoretical advances have been made in the prediction of simple relationships and the overall pictures for the coil–stretch transition[3-5] and polymer fracture.[6-9] However, analytical treatments and direct computation are not usually sufficient when one wishes to consider a variety of complicating aspects, ranging from the hydrodynamic interaction (HI) effects in polymer dynamics to the nonlinear nature of macromolecular chains.[10,11] In this regard, an appealing alternative which has been gaining popularity in the past years is the computer simulation of the Brownian dynamics of the chain. The simulation is made from the very first principles of Brownian motion and can be applied to problems of arbitrary complexity, both in the polymer model and in the solvent flow as well. The technique has been employed in a number of studies in shear flows,[12-19] while its use in the study of polymer conformation[19] and fracture[20] has been less frequent.

A relevant problem is that regarding the mechanical model employed to represent the polymer chain. The bead-and-spring model, or Rouse[21] chain is used very often in polymer dynamics because of its tractability. However, for problems with solvent flow, it presents the drawback that the chain is infinitely stretchable. A model with finitely extensible, nonlinear elastic (FENE) springs[11,22] is a common alternative.[5,20] However, the property of the FENE spring of being able to support an indefinitely large tension with finite elongation, without breaking, does not seems to be a good representation of the real behavior of a segment in a polymer chain. The Kramers[23] freely jointed chain of beads and rods is quite useful in several aspects,[19] but suffers from the same limitation.

In this paper, we study a chain model having beads connected by springs that obey a Morse potential. At low energies, i.e., in weak flows, the Morse springs execute small-amplitude oscillations about the equilibrium length, like a Fraenkel spring,[11] and the model is similar to the Kramers freely jointed chain. On the other hand, in strong flows, if a spring obtains a given finite energy, it breaks. The Morse potential is indeed used in other grounds to represent both small-amplitude vibrations as well as dissociation of chemical, covalent bonds. Our model is similarly expected to represent steady-state properties and polymer fracture. Our second model is the Rouse chain. Being aware of its limitation, we consider the Rouse chain as a useful tool, first, for checking the performance of the simulation procedure by comparison with known results, and second, to provide a

[a] To whom correspondence should be addressed.

reference for the discussion of the results of the other model (the Morse chain), which is substantially different.

We also pay attention for both models to the effect of hydrodynamic interactions (HI). It is well known that the dynamics of polymer chains in a quiescent solvent is influenced strongly by the HI effects, which modifies even the exponents in the scaling laws for properties vs molecular weight. On the other hand, in some aspects of flowing polymer solutions, HI has simply a quantitative influence, but it does not determine the overall behavior.[5,18] The study of HI effects for polymers under flow may be relevant for further theoretical and simulation studies, which may be simplified greatly if such effects could be neglected.

We present in this paper a Brownian dynamics simulation study or Rouse chains and Morse chains of varying length, with and without hydrodynamic interaction effects, in steady elongational flow of the uniaxial type. Simulations are carried out at different elongational rates, which allow us to discuss how the polymer coil unravels in the flow, as manifested by its varying conformation. The true breakage behavior of the Morse chains and the critical (diverging) behavior of Rouse chains allows the characterization of the minimum elongation rate for polymer fracture. These results are of relevance as the starting point for future studies of fracture kinetics and size distribution of the fragments.

THEORY AND METHODS

Elongational flow

We consider a dilute polymer solution subjected to a steady elongational flow of the uniaxial type. The solvent velocity at a point with position vector $\mathbf{r}$ is

$$\mathbf{v}(\mathbf{r}) = \varkappa \cdot \mathbf{r}, \tag{1}$$

where the velocity gradient $\varkappa$ is given by

$$\varkappa = \begin{pmatrix} -1/2 & 0 & 0 \\ 0 & -1/2 & 0 \\ 0 & 0 & 1 \end{pmatrix} \dot{\epsilon} \tag{2}$$

in terms of the elongational rate $\dot{\epsilon}$. In this flow, the origin is a stagnation point. Following previous calculations and simulations,[5,18] we have considered only the case of positive $\dot{\epsilon}$. As kindly pointed out by a referee of this paper, our simulation program could be applied without change for negative $\dot{\epsilon}$, thus covering the less common case of biaxial stretching flow.

The elongational viscosity $\bar{\eta}$ is expressed from the stress tensor τ as[11]

$$\tau_{zz} - \tau_{xx} = -\bar{\eta}\dot{\epsilon}. \tag{3}$$

According to Trouton law, at low rates the elongational viscosity of the solvent is $3\eta_s$, where η_s is its zero-shear-rate viscosity. In a polymer solution, the excess stress tensor due to the polymer chains is denoted as τ_p and the increase in elongational viscosity of the solution with respect to the solvent is

$$\bar{\eta} - 3\eta_s = -(\tau_{zz} - \tau_{xx})_p/\dot{\epsilon}. \tag{4}$$

By analogy with shear flows, we employ an intrinsic elongational viscosity given by

$$[\bar{\eta}] = (\bar{\eta} - 3\eta_s)/3\eta_s c \tag{5}$$

in the limit of zero polymer concentration c. At very low elongational rate, $[\bar{\eta}]$ coincides with the zero-shear-rate viscosity.

Models

A polymer chain is modeled as a string of N spherical elements, or beads of radius σ joined by $N - 1$ connectors. We denote as $\mathbf{r}_i$ the position vector for the beads ($i = 1,...,N$), so that the bond vectors associated to the connectors are given by

$$\mathbf{Q}_j = \mathbf{r}_j + 1 - \mathbf{r}_j \tag{6}$$

for $j = 1,...,N - 1$. Although the two models considered in this work differ in the nature of the connectors, in both of them the orientations of the bonds are independent. As a consequence, if $l \equiv \langle Q_j^2 \rangle$ is the root-mean-square bond length, then the mean square end-to-end distance $\langle r^2 \rangle_0$ is given by

$$\langle r^2 \rangle_0 = (N - 1)l^2. \tag{7}$$

The friction coefficient of the beads is $\zeta = 6\pi\eta_0\sigma$. If the results are expressed in a conveniently normalized form (see below), they are independent of the choice of σ or ζ when the hydrodynamic interaction is neglected. In any case, we use in the simulations $\sigma = 0.256b'$, where b' is the characteristic bond length of the model. This corresponds to a commonly used value for the hydrodynamic interaction parameter[10] $h^* = 0.25$ (see Ref. 11, pp. 169, 170).

For a chain of elastic springs, the contribution of the n polymer molecules to the stress tensor is (Ref. 11, Table 15.2-1)

$$\tau_p = -n \sum_j \langle \mathbf{F}_j^{(c)} \mathbf{Q}_j \rangle + (N - 1)nk_BT\mathbf{1}, \tag{8}$$

where $\mathbf{F}_j^{(c)}$ is the connector force (not to be confused with the frictional force). Then, from Eqs. (4), (5), and (8), the elongational intrinsic viscosity is calculated as

$$[\bar{\eta}] = -(N_A/3\eta_s M\dot{\epsilon}) \sum_j (\langle F_j^z Q_j^z \rangle - \langle F_j^x Q_j^x \rangle). \tag{9}$$

The above results apply to the two types of chain models considered in this work. We now describe their specific features. One of the models is the Rouse chain,[21] in which the bonds connecting the beads are Hookean springs with a stretching force $\mathbf{F}_j = -H\mathbf{Q}_j$, where H is the force constant. A characteristic time for the Rouse chain is defined as

$$\lambda_H = \zeta/4H = \pi\eta_s\sigma b'^2/2k_BT, \tag{10}$$

where $b' \equiv l$. As is well known, the Hookean forces result in a Gaussian distribution for all the intrachain distances, including the $\mathbf{Q}_j$ and the end-to-end distance.

For a Rouse chain, Eq. (8) takes a simpler form,

$$\tau_p = -nH \sum_j \langle Q_j Q_j \rangle + (N - 1)nk_BT\mathbf{1} \tag{11}$$

and Eq. (9) simplifies similarly.

The second model considered, which we call the Morse chain, is intended to remove some of the unphysical properties of the Rouse chain. In this model, the potential energy for bond stretching is the Morse potential

$$V_j = A(1 - e^{-B(Q_j - b)})^2, \qquad (12)$$

where b is now the equilibrium length and A and B are constants of the model. The instantaneous spring length may take any value from 0 to ∞. For low energies, the connectors behave as stiff springs that perform small amplitude vibrations and the model resembles a freely jointed chain of segments with length b. The stretching force, obtained as the derivative of Eq. (12),

$$F_j = -2ABe^{-B(Q_j - b)}(1 - e^{-B(Q_j - b)}) \qquad (13)$$

varies nonlinearly with the bond length and finally the bond breaks when its potential reaches the dissociation energy A. In Fig. 1, we plot the connector force vs the connector length for the two models, along with that for another common model, the FENE spring,[11,22] so that the differences can be appreciated.

Actually, we made some simulations[24] with a Lennard-Jones potential between beads (as in our study of shear flows[18]) intended to represent excluded volume effects. The simulation were very costly and the results, apart from obvious quantitative differences, did not show differences in qualitative aspects and trends. Therefore we just present here results obtained without excluded volume.
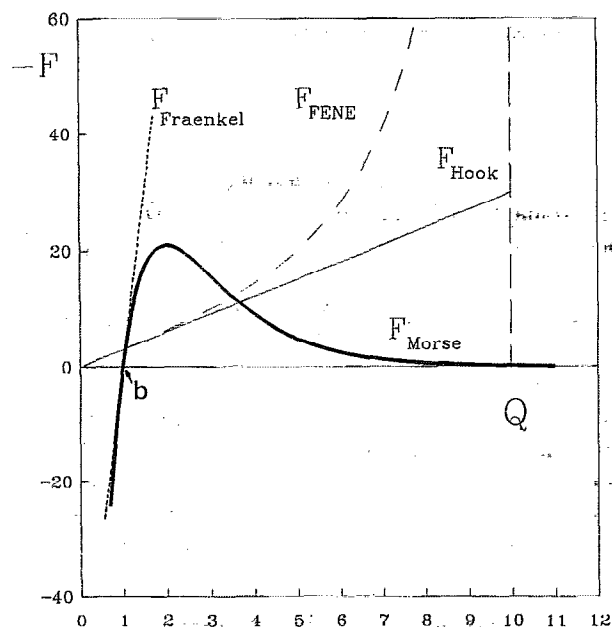

FIG. 1. A plot of the connector force vs connector length. The thin line is for the Rouse chain (Hookean connector). The thick line is for the Morse chain with $A = 60$, $B = 0.7$, and $b = 1$. b is marked as the distance for which $F = 0$ and F_{max} takes place at $Q = AB/2$. The dashed line is for a FENE chain with maximum elongation $Q_0 = 10$ (all the parameters are in dimensionless form). The dotted line is for a Fraenkel spring with a force constant equal to $2AB^2$.

Brownian dynamics simulation

Brownian trajectories of the chains are simulated in the computer using the first-order algorithm of Ermak and MacCammon[25] with a second-order modification.[26] In the former version, the position vector of a bead is obtained from the initial position r_i^0 after a Brownian step of duration Δt as

$$r_i = r_i^0 + (\Delta t/kT) \sum_k D_{ik}^0 \cdot F_k^0 + \Delta t v(r_i^0) + \rho_i^0. \qquad (14)$$

The superscript 0 in r_i^0 and elsewhere refers to the instant at which the time step begins. D_{ik}^0 ($i,k = 1,...,N$) is the ik block of the diffusion tensor. F_k^0 is the spring force on bead k: $F_k^0 = -F_k^{(c)} + F_{k-1}^{(c)}$ except for $F_1^0 = -F_1^{(c)}$ and $F_N^0 = F_{N-1}^{(c)}$. ρ_i^0 is a random vector with covariance equal to $2\Delta t D_{ik}^0$. When we consider hydrodynamic interaction between the chain units, the Rotne–Prager–Yamakawa interaction tensor is used for D_{ik}^0. If hydrodynamic interaction is neglected, Eq. (14) takes a simpler form

$$r_i = r_i^0 + (\Delta t/\zeta) F_k^0 + \Delta t v(r_i^0) + \rho_i^0. \qquad (15)$$

Further details about the Brownian simulations are as in our previous papers.[16-18]

Dimensionless quantities

In the simulation work and in the presentation of results, it is useful to employ nondimensional quantities. This is accomplished dividing the basic quantities by the following factors: length b' (with $b' \equiv l$ for the Rouse model and $b' \equiv b$ for the Morse chain); force $k_B T$; and time $\zeta b'^2/k_B T$. In these units, the characteristic time of the Rouse chain is $\lambda_H = 1/12$. Thus the reduced elongational rate would be $\dot{\epsilon}^* = (\zeta b'^2/k_B T)\dot{\epsilon}$. In some instances, it is preferrable to reduce the elongational rate using a factor that depends on polymer length. Concretely we employ the reduced rate ν defined by

$$\nu = (M\eta_s[\eta]_0/RT)\dot{\epsilon}. \qquad (16)$$

We normalize the intrinsic viscosity as

$$[\bar{\eta}]^* = [\bar{\eta}]M^3/N_A b, \qquad (17)$$

while other workers[11] prefer to express the excess viscosity as

$$(\bar{\eta} - 3\eta_s)^* \equiv (\bar{\eta} - 3\eta_s)/nk_B T = [\bar{\eta}]^* \qquad (18)$$

and sometimes it is presented as the ratio

$$\frac{(\bar{\eta} - 3\eta_s)}{3(\eta_0 - \eta_s)} = \frac{[\bar{\eta}]}{[\eta]_0} = \frac{[\bar{\eta}]^*}{[\eta]_0^*}. \qquad (19)$$

With reduced quantities, the reduced rate is given by

$$\nu = ([\eta]_0^*/6\pi\sigma^*)\dot{\epsilon}^*. \qquad (20)$$

Hereafter, the elongational rate will be generically denoted as $\dot{\epsilon}$ and we will use $\dot{\epsilon}^*$ when we refer specifically to the dimensionless form.

Simulation procedure

The Brownian trajectory of a polymer chain was started from a random conformation generated by a simple Monte

Carlo procedure in conditions corresponding to the absence of flow. Then a very large number of simulation steps (typically 1.5×10^6) of length $\Delta t = 0.01$ (Rouse) or 0.002 (Morse) were taken. The moving averages needed for the calculation of the properties were monitored. During the first part of the trajectory, the averages increased from the no-flow values to reach the steady-state values. That part of the trajectory comprising about 5×10^5 steps was rejected and the averages were recalculated for the remaining portion, where the chain is equilibrated with the flow.

The choice of the time step Δt is a delicate point in Brownian dynamics simulation due to the compromise between discretization and trajectory length. Our value for Rouse chains $\Delta t = 0.01$ has been already proven to be effective.[17] Anyhow, we checked (for both models) that halving Δt and doubling the number of steps did not produce changes in the results significantly over the statistical uncertainties. This is in part due to the robustness of the second-order algorithm,[26] which allows longer steps than the Ermak–McCammon algorithm. The good agreement discussed below of Brownian dynamics simulation with all the available analytical or Monte Carlo results is a definitive check of our simulation procedure.

For the parameters in the Morse potential, we take first $A = 60$ in units of kT. This dissociation energy is of the same order as the typical values for true chemical bonds. Second, we use $B = 0.7$, which is chosen so that the mean length l of the springs is only about 5% larger than the equilibrium length b. In regard to the Rouse model, the reduced value for the force constant is $H = 3$.

RESULTS AND DISCUSSION

Chain dimensions and conformation

One of the few analytical results for properties of polymer chains in elongational flow is the equation of Bird et al.[27] for the end-to-end distance of Rouse chains in the absence of HI

$$\frac{\langle r^2 \rangle}{\langle r^2 \rangle_0} = 1 + \frac{2\lambda_H^2 \dot{\epsilon}^2}{N(N+1)}$$

$$\times \sum_{\substack{m=1 \\ odd}}^{N-1} \frac{\cos^2 M}{\sin^2 M(\sin^2 M + \lambda_H \dot{\epsilon})(\sin^2 M - \lambda_H \dot{\epsilon})},$$

$$(21)$$

where $M = (m\pi/2N)$

Our results for $\langle r^2 \rangle$ without HI for the Rouse chains (not shown) were found to be in excellent agreement, within a few percent, with Eq. (21). This confirms the validity of the simulation algorithm and the working conditions. According to Eq. (21), there is a critical rate $\dot{\epsilon}_c$ at which the polymer dimensions increase indefinitely, as shown in Fig. 2. From Eq. (21), the critical rate for uniaxial flow is

$$\dot{\epsilon}_c = \lambda_H^{-1} \sin^2(\pi/2N) \qquad (22a)$$

$$= (\pi^2/4\lambda_H)N^{-2} \quad (N \to \infty). \qquad (22b)$$

Simulation results for Rouse chains with HI are also shown in Fig. 2. We note that for chains long enough $(N > 3)$, $\langle r^2 \rangle_{HI}$ is smaller than $\langle r^2 \rangle_{no\ HI}$. In other words, when HI is considered, the expansion in polymer dimensions due to the flow is not as great as that predicted when HI is neglected. This HI effect in elongational flows is in the same direction as that found for shear flows.[17,28] The HI/no HI ratios can be substantially different from unity, essentially because $\dot{\epsilon}_c$ is different. It is noteworthy that the HI effect for very short chains $(N = 2,3)$ is the opposite. This also happened in the case of shear flows[16,17] and illustrates that the use of the simplistic dumbbell model may be misleading, even for rough estimation. Summarizing the HI effects on polymer dimensions, we note that HI does not introduce qualitative differences in the behavior of $\langle r^2 \rangle$ vs $\dot{\epsilon}$ with just a noticeable decrease in dimensions for a given $\dot{\epsilon}$ and an increase in the elongational rate required for critical behavior.

Simulation results for Morse chains with the parameters given above are presented in Fig. 3. The HI effect is again to decrease the elongational power of the flow. For instance, for $N = 20$ with $\langle r^2 \rangle_0 = 22$, when $\dot{\epsilon}^* = 0.1$ (which is at most half of the fracture limit $\dot{\epsilon}_f$; see below), we have $\langle r^2 \rangle_{no\ HI} \cong 170$, while $\langle r^2 \rangle_{HI} \cong 60$. There is a distinction between the $\dot{\epsilon}$ dependence of the dimensions of Rouse and Morse chains for large N. While for the Rouse model the dimensions diverge asymptotically, for the Morse chain the trend indicates an incipient sigmoidal shape (compare the $N = 20$ data in Figs. 2 and 3) which is interrupted at some particular $\dot{\epsilon}$. Above this point, a steady state cannot be reached.
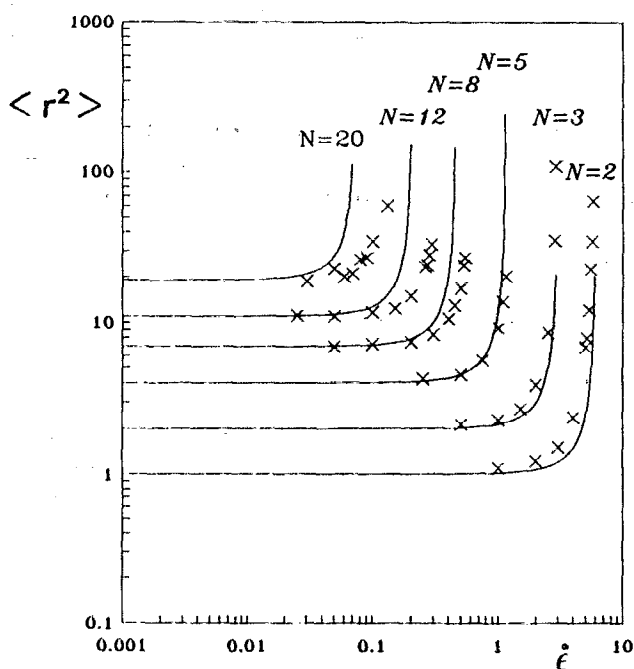

FIG. 2. Values of $\langle r^2 \rangle$ for Rouse chains with different length vs the elongational rate $\dot{\epsilon}$. (—) is the analytical results without HI from Eq. 21. ($\times$) is the simulation results with HI (the HI conditions are always the Rotne–Prager–Yamakawa tensor and $h^* = 0.25$). All the sets of data points terminate at $\dot{\epsilon}_c$.
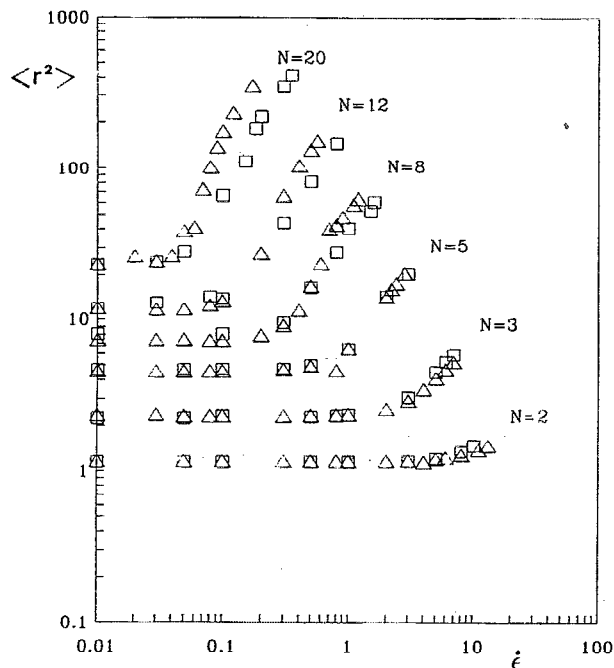
FIG. 3. Values of $\langle r^2 \rangle$ for Morse chains with different length vs the elongational rate $\dot\epsilon$. ($\triangle$) no HI; ($\square$) HI. All the sets of data points terminate at $\dot\epsilon_c$.
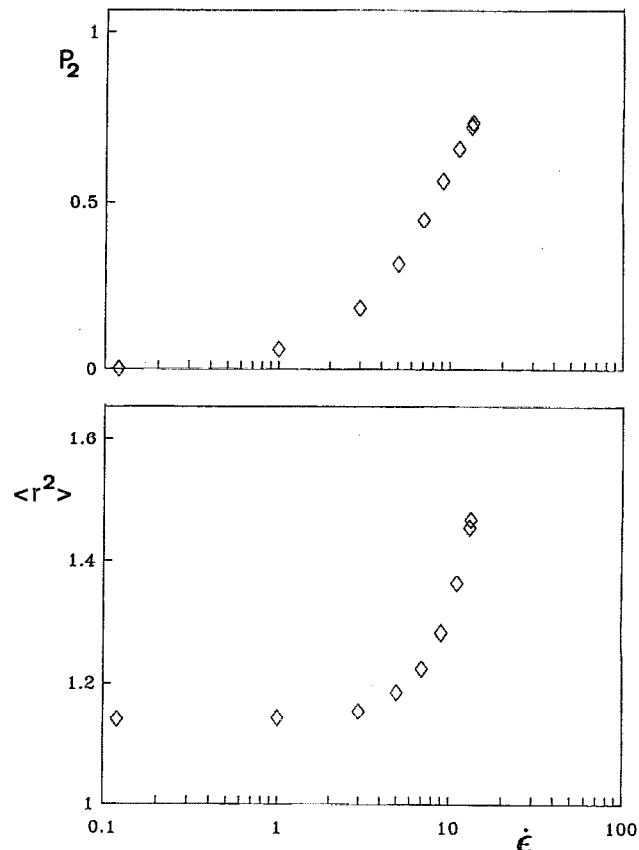

FIG. 4. End-to-end distance $\langle r^2 \rangle$ and order parameter $P_2 \equiv \langle P_2 (\cos\beta) \rangle$ for a Morse dumbbell ($N = 2$) without HI vs $\dot\epsilon$.

The behavior of the Morse chain can be better understood regarding the situation for the single spring of a dumbbell. If the dumbbell is oriented, making an angle β with the elongation axis (z), then the tension force in the spring due to the flow is $\zeta Q \dot\epsilon P_2 (\cos\beta)$, where P_2 is the second Legendre polynomial. If the flow is strong enough, the dumbbell will be nearly aligned with z and, roughly, $P_2 \cong 1$. Obviously, at larger $\dot\epsilon$, the force in the spring is larger. However, there is a maximum force that a Morse spring can withstand, corresponding to the maximum in the F curve in Fig. 1. The maximum value is $F_{max} = AB/2$ and takes place for $Q_{max} = b + \ln 2/B$. Thus, the maximum elongational rate is

$$\dot\epsilon_f = F_{max}/\zeta Q_{max} \qquad (23a)$$

$$= AB/[2\zeta(b + \ln 2/b)P_2] \quad \text{(for } N = 2). \quad (23b)$$

For $\dot\epsilon > \dot\epsilon_f$, the spring cannot withstand the force due to the flow. No steady state is reached and the spring breaks. Thus $\dot\epsilon_f$ determines the fracture limit. Numerical results for the Morse dumbbell with $A = 60$, $B = 0.7$, and $b = 1$ are given in Fig. 4. The highest elongational rate reachable in the simulation is $\dot\epsilon_f^* = 13.2$, in reduced units. The prediction from Eq. (23) with $P_2 = 0.74$ (see Fig. 4) is 14.2, in very good agreement.

Quantitative predictions are not possible for long chains, since we do not know a priori (without simulation) some aspects such as polymer orientation and the distribution of the elongational stress along the chain. In any case, there is a limiting $\dot\epsilon_f$ for each value of N that can be determined carrying out simulations at varying $\dot\epsilon$; if $\dot\epsilon > \dot\epsilon_f$, there is simply a computational overflow.

A more complete description of the conformation of the Morse chains in elongational flow can be made analyzing, together with $\langle r^2 \rangle$, other quantities determined by bond stretching and alignment. Thus, for $N = 20$, we present in Fig. 5 results for the rms bond lengths $\langle Q_{10}^2 \rangle$, $\langle Q_5^2 \rangle$, and $\langle Q_2^2 \rangle$, corresponding to bonds 10 (central), 5 (at one quarter of contour length), and 2 (second from the end), as well as the order parameters $\langle P_2 (\cos\beta_{10}) \rangle$, $\langle P_2 (\cos\beta_5) \rangle$, and $\langle P_2 (\cos\beta_2) \rangle$ that measure the average alignment of the individual bonds with respect to the flow. [The solution birefringence[29,30] would be given by an average of $\langle P_2 (\cos\beta_j) \rangle$ over the bonds j.] The results in Fig. 5 are from simulations without HI. It is clear that apart from quantitative differences, the trend observed with HI should be the same. These results complement those displayed in Fig. 4 for the lowest N.

Relevant conclusions about the transition (with increasing $\dot\epsilon$) from the coiled state to the stretched one can be drawn from Figs. 4 and 5. Essentially, we note that the large increase in polymer dimensions, as measured by $\langle r^2 \rangle$, is not due to bond stretching, since the $\langle Q_j^2 \rangle$'s increase 50% at most, but instead is due to the unfolding of the coil, as revealed by the increase in the $\langle P_2 \rangle$ values. This increase is important itself, since it determines the onset of birefringence which is observed experimentally.[29,30] Therefore, the so-called coil–stretch transition (in the variation of proper-
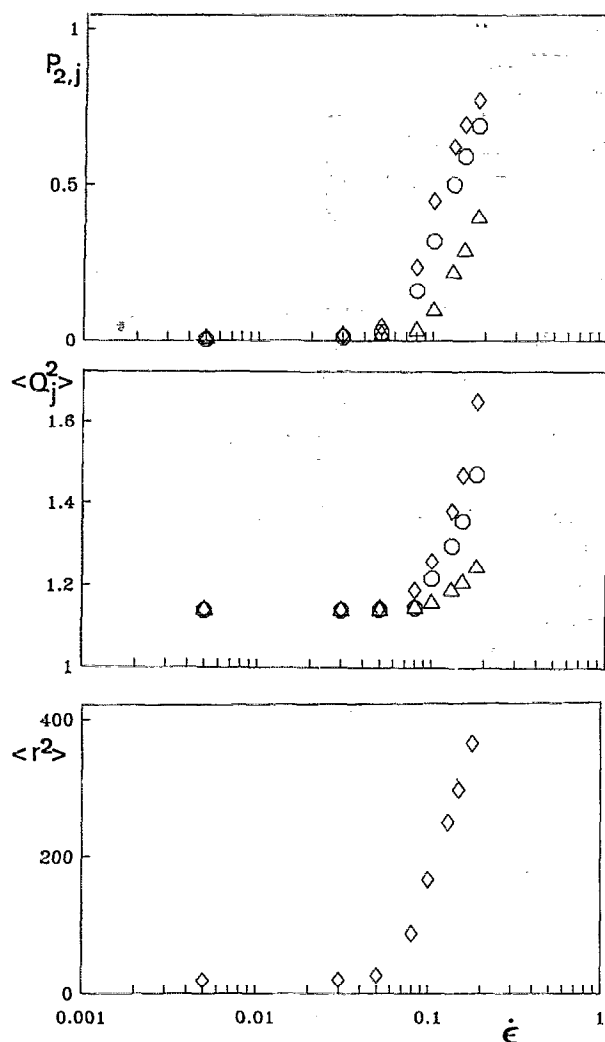
FIG. 5. End-to-end distance $\langle r^2 \rangle$, order parameters $P_{2,j} \equiv \langle P_2 (\cos\beta_j) \rangle$, and mean square connector lengths $\langle Q_j^2 \rangle$ for various bonds $j = 10$, 5, and 2 of a Morse chain without HI vs $\dot{\epsilon}$.

$j = 10, 5,$ and 2 ($j/N = 0.5, 0.25,$ and 0.1), we note that the alignment of bonds 10 and 5 proceeds at nearly the same pace, while that of bond 2 begins at nearly the same $\dot{\epsilon}$, but is not so pronounced. Since we are not dealing with very long chains, we do not feel sure about whether this is an indication of the yo-yo mechanism, or just a spurious end effect.

We wish to point out (because there is some confusion in this regard in the literature) that the coil–stretch transition has been considered here in the elongational-rate dependence of the steady-state properties. A related, but not necessarily equivalent point of view is the dynamic one, based on the time dependence of the properties after the inception of the flow. This is the direction followed in previous work[5] and in the other part of our study.[24]

Elongational viscosity

We obtained the elongational viscosity of the two models as a function of $\dot{\epsilon}$ and for various N, both without and with HI. The only previous analytical result of which we are aware is the equation of Bird *et al.*[11] for the Gaussian or Rouse dumbbell ($N = 2$) without HI

$$[\bar{\eta}]^* = \frac{6\pi\sigma\lambda_H}{(1 - 2\lambda_H\epsilon)(1 + \lambda_H\epsilon)}, \tag{24}$$

where all the quantities are in dimensionless form and $\lambda_H = 1/12$. Our results were found to be in excellent agreement with Eq. (24), as shown in Fig. 6, where results for other N's are displayed. We note again the critical behavior of the Rouse model at $\dot{\epsilon}_c$. The results with HI showed a
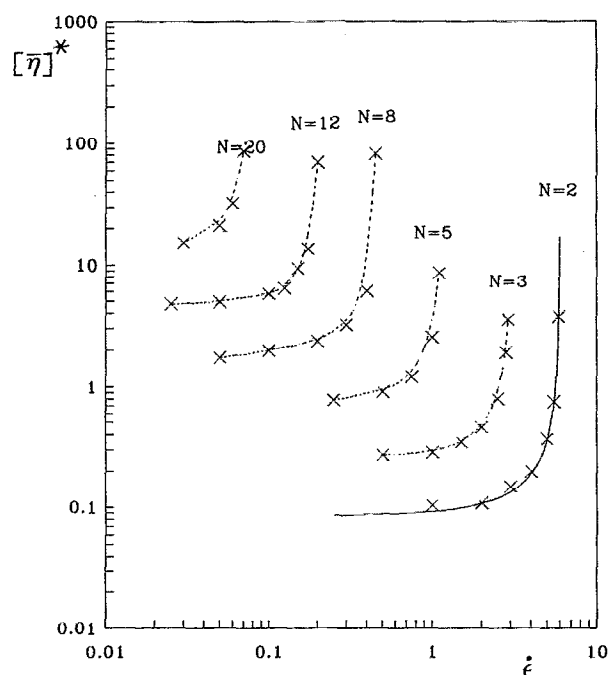
ties with $\dot{\epsilon}$) is due to the orientation of the polymer segments in the direction of the flow. This picture is consistent with that found by Liu[19] in his study of FENE chains.

We note that the order parameters and $\langle r^2 \rangle$ begin to grow at an elongation rate quite smaller than $\dot{\epsilon}_f$; for instance, for $N = 20$, the onset of that increase is at about $\dot{\epsilon}^* \cong 0.05$, while $\dot{\epsilon}_f^* \cong 0.18$. Thus the transition takes place over a broad range of $\dot{\epsilon}$. For $N = 20$, the transition does not seem to be sharper that that for $N = 2$. With our results, we cannot establish a definite, critical value $\dot{\epsilon}_c$ for the Morse chain that would characterize the coil–stretch transition. Only the elongational rate for fracture $\dot{\epsilon}_f$ is well defined for Morse chains. We do not see evidence for the type of transition predicted by de Gennes,[3] which was not found either in a recent study of Kramers freely jointed chains.[5] It is tempting to employ our simulation results to test the "yo-yo" hypothesis[4] for the transition, which states that unfolding begins at the very center of the chain, while the ends remain rather coiled. Comparing the results in Fig. 5 for the various bonds

FIG. 6. Elongational intrinsic viscosity $[\eta]^*$ for Rouse chains of different length vs $\dot{\epsilon}$ (results without HI). ($\times$) is the simulation results. (—) is the analytical result [Eq. (24)] for the dumbbell ($N = 2$). The dotted lines just trace the trend of the data points.

completely similar trend. For $N > 3$, $[\bar{\eta}]_{HI} < [\bar{\eta}]_{no\ HI}$ and $\dot{\epsilon}_{c,HI} > \dot{\epsilon}_{c,no\ HI}$.

A parallel treatment was carried out for the Morse chains. The aspect of the variation of $[\bar{\eta}]$ with $\dot{\epsilon}$ is completely similar to that of $\langle r^2 \rangle$, both with and without HI.

As commented above, at low elongational rates, the elongational intrinsic viscosity should coincide with the zero-shear intrinsic viscosity. The latter can be evaluated analytically in the no HI case,[11] or the using the so-called rigid-body Monte Carlo treatment for chains with HI.[31-33] Then we compared our Brownian dynamics simulation results for $[\bar{\eta}]$ at low $\dot{\epsilon}$ with these alternative values of $[\eta]_0$. It must be recalled in this context that at low flow rates, the Brownian dynamics results for the viscosity are influenced largely by statistical errors [in such conditions, the right-hand side of Eq. (4) implies a difference between two very close values, which amplifies the simulation errors; this has been discussed already[16]]. Anyhow, the agreement in the comparison was good within the large uncertainties.

As is done in the study of shear flows, the dependence of properties on flow strength can be analyzed employing the zero-rate viscosities in terms of the rate constant ν that combines $\dot{\epsilon}$ and $[\eta]_0$, formulated in Eqs. (16) and (20). Examples of this situation are given in Fig. 7 for Rouse chains with HI and in Fig. 8 for Morse chains without HI. In the other

two cases, the trend of the results is similar. The main point in this type of representation is whether the results for various chain lengths cluster together, following a length-independent variation with ν. We note that this behavior is followed only qualitatively. Thus we note that the departure of the properties from the zero-flow values takes place very roughly at $\nu \cong 1$. One could conclude the existence of a critical ν_c for the coil–stretch transition that would be close to that value. Regardless of the numerical value of ν_c, the scaling law $[\eta]_0 \propto M^{1/2}$ for the intrinsic viscosity in theta chains (with $N \propto M$) would lead to $\dot{\epsilon}_c \propto M^{-3/2}$, as is indeed observed experimentally.[1,6] The statistical quality of our data and mostly the short length of the chains simulated do not allow quantitative conclusions in this regard.

Power law for the critical elongational rate for polymer fracture

As commented above, the critical elongational rate at which the polymer chain breaks $\dot{\epsilon}_f$ is well defined and has been obtained in our simulations. Results are presented in a log–log plot vs N in Fig. 9, from which we can ascertain the possible power laws expressing the length, or molecular
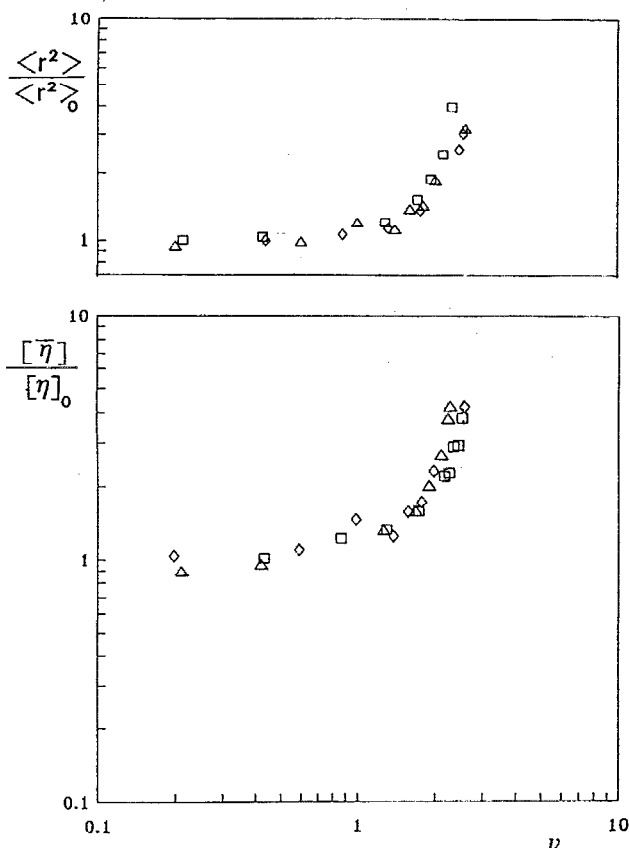

FIG. 7. Ratios of $\langle r^2 \rangle$ and $[\eta]$ to the values at zero-rate flow for Rouse chains with HI. ($\square$) $N = 8$; ($\triangle$) $N = 12$; ($\lozenge$) $N = 20$.
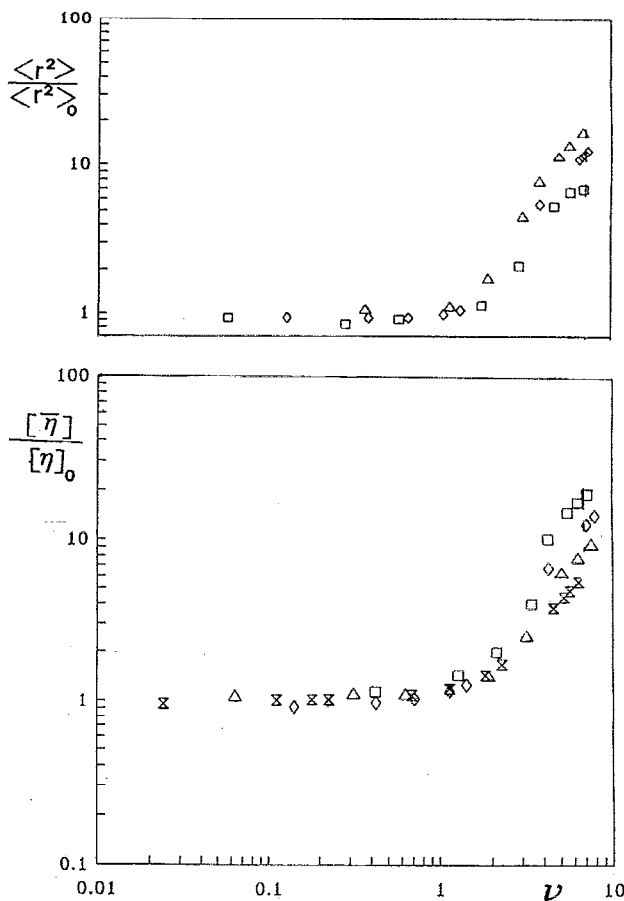
FIG. 8. The same as in Fig. 7 for Morse chains without HI. Note that for a different model with different HI conditions, the aspect of the data is similar to that in Fig. 7.
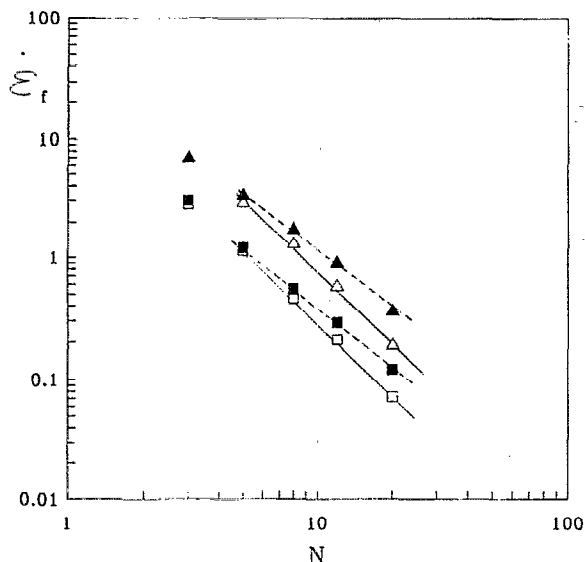
FIG. 9. Values of $\dot{\varepsilon}_c$ (Rouse model) and $\dot{\varepsilon}_f$ (Morse chain) vs chain length N ($\square$) Rouse, without HI; ($\blacksquare$) Rouse, with HI; ($\triangle$) Morse, without HI; ($\blacktriangle$) Morse, with HI. The straight lines are those obtained to deduce the scaling laws.

weight dependence of $\dot{\varepsilon}_f$. For the Rouse chain without HI, we find $\dot{\varepsilon}_f \propto N^{-1.98}$ and for the Morse chain without HI, the result is $\dot{\varepsilon}_f \propto N^{-1.97}$. Thus for both models without HI, our results suggest a scaling law $\dot{\varepsilon}_f \propto M^{-2}$. Indeed this dependence has been observed experimentally by Keller and co-workers[1,6] (these authors used a cross-slots device for degradation experiments of polystyrene solutions in decaline that they claim to be dilute by any criteria). Anyhow, we should note that there is some controversy about the influence of the nature of the elongational flow on the scaling law.[34]

On the other hand, when HI is included, as it should, our results (see Fig. 9) are $\dot{\varepsilon}_f \propto N^{-1.65}$ for Rouse chains and $\dot{\varepsilon}_f \propto N^{-1.60}$ for Morse chains, in disagreement with the observations. At first sight, it was paradoxical that the proper inclusion of hydrodynamic interaction would destroy the agreement with experimental result. Odell et al.[6] have reported a simple argument that gives a prediction of the scaling law. The polymer chain is supposed to be unraveled, in a linear conformation along axis z, before it breaks, but with connectors not appreciably stretched. Brownian motion can be approximately neglected in strong flow, so that the bead velocities are $u_i = 0$. The unperturbed (by HI) solvent velocity is $v_i^0 = \dot{\varepsilon} z_i$, where $z_i = b(2i - N - 1)/2$. Then the relative bead velocity is

$$u_i - v_i^0 = \dot{\varepsilon} b(2i - N - 1)/2. \qquad (25)$$

The drag force at each bead is $F_i^{(h)} = -\zeta(u_i - v_i^0)$ and the total tension in the chain $F = \Sigma_i F_i^{(h)}$ is found to be $F = \dot{\varepsilon} b N^2/8$ for high N. For the critical fracture rate $\dot{\varepsilon}_f$, F reaches the value needed for the breakage of a connector F_{max}. As b and F_{max} are given constants, the argument of Odell et al.[6] gives finally $\dot{\varepsilon}_f \propto N^{-2}$.

We undertook a similar prediction including HI. Employing a rigorous Kirkwood–Riseman formalism,[32,35,36] the drag forces at the beads are instead

$$\mathbf{F}_i^{(h)} = -\sum_k \mathbf{C}_{ik}(\mathbf{u}_k - \mathbf{v}_k^0), \qquad (26)$$

where $\mathbf{C}_{ik}$ is the ik 3×3 block of a friction supermatrix of dimension $3N \times 3N$ $\mathscr{C}$ given as $\mathscr{C} = \mathscr{B}^{-1}$, where the ik blocks of the mobility supermatrix $\mathscr{B}$ are

$$\mathscr{B}_{ik} = \zeta^{-1}\delta_{ik}\mathbf{1} + (1 - \delta_{ik})\mathbf{T}_{ik}. \qquad (27)$$

In Eq. (27), δ_{ik} is Kronecker's delta and $\mathbf{T}_{ik}$ is a hydrodynamic interaction Oseen tensor. Further details can be found elsewhere.[35-37] An analytical treatment of Eqs. (25)–(27) for large N leads to the final result that the total force depend on N as $F \propto N^2/\ln N$. Thus the correction with respect to the no HI case is just a $\ln N$ factor. The same logarithmic correction happens in the case of translational and rotational friction coefficients and intrinsic viscosities of rods.[37] Then, our result for the fracture rate, considering HI, is

$$\dot{\varepsilon}_f \propto N^{-2}\ln N. \qquad (28)$$

When the chain is very long, the logarithmic term varies with N much slower than N^{-2}, so that over a discrete range of chain length, the effective scaling law must be $\dot{\varepsilon}_f \propto N^{-2}$ or M^{-2}. We have also solved numerically Eqs. (25)–(27), using standard computer algorithms with HI[35-37] as a function of N. A log–log plot of the numerical $\dot{\varepsilon}_f$ values vs N shows a slope of about 1.6, which explains the slope found in Fig. 9 for the Brownian dynamics simulation results with HI. For N as high as 500, the observed slope is 1.8, which is still somewhat far from the limiting value. Therefore, the discrepancy was due to the shortness of the simulated chains, which is unavoidable due to limitations in computational resources. Anyhow, we have been able to conclude that $\dot{\varepsilon}_f \propto M^{-2}$ both for Rouse chains as well as for Morse chains. This theoretical result is valid rigorously when hydrodynamic result is neglected and effectively when hydrodynamic interaction is included.

ACKNOWLEDGMENTS

[1] A. Keller and J. A. Odell, Colloid Polym. Sci. 263, 181 (1985).
[2] Polymer-Flow Interaction, edited by Y. Rabin (American Institute of Physics, New York, 1986).
[3] P. G. De Gennes, J. Chem. Phys 60, 5030 (1974).
[4] G. Ryskin, J. Fluid Mech. 178, 423 (1987); Phys. Rev. Lett. 59, 2059 (1987).
[5] J. M. Wiest, L. E. Wedgewood, and R. B. Bird, J. Chem. Phys. 88, 4022 (1989).
[6] J. A. Odell and A. Keller, J. Polym. Sci. Polym. Phys. Ed. 24, 1889 (1986).
[7] Y. Rabin, J. Chem. Phys. 86, 5215 (1987); J. Non-Newtonian Fluid Mech. 30, 119 (1988).
[8] Y. Rabin, J. Chem. Phys. 88, 4014 (1988).
[9] J. A. Odell, A. Keller, and Y. Rabin, J. Chem. Phys. 88, 4022 (1988).
[10] H. Yamakawa, Modern Theory of Polymer Solutions (Harper and Row, New York, 1971).
[11] R. B. Bird, C. F. Curtiss, O. Hassager, and R. C. Armstrong, Dynamics of Polymeric Liquids, 2nd ed. (Wiley, New York, 1987), Vol. 2.

[12] Dotson, P. J., J. Chem. Phys. **79**, 5730 (1983).

[13] H. H. Saab and P. J. Dotson, J. Chem. Phys. **86**, 3039 (1987).

[14] H. C. Ötinger, J. Chem. Phys. **84**, 1850 (1986).

[15] W. Zylka and H. C. Öttinger, J. Chem. Phys. **90**, 474 (1989).

[16] F. G. Diaz, J. Garcia de la Torre, and J. J. Freire, Polymer **30**, 259 (1989).

[17] J. J. Lopez Cascales and J. Garcia de la Torre, Macromolecules **23**, 809 (1990).

[18] J. J. Lopez Cascales and J. Garcia de la Torre, Polymer **00**, 00 (1991).

[19] T. W. Liu, J. Chem. Phys. **90**, 5826 (1989).

[20] H. R. Reese and B. H. Zimm, J. Chem. Phys. **92**, 2650 (1990).

[21] P. E. Rouse, J. Chem. Phys. **21**, 1272 (1953).

[22] H. R. Warner, Ind. Eng. Chem. Fundam, **11**, 379 (1972).

[23] H. A. Kramers, Physica **11**, 1 (1944).

[24] J. J. López Cascales, Ph.D. thesis, Universidad de Murcia, 1991.

[25] D. L. Ermak and J. A. McCammon, J. Chem. Phys. **69**, 1352 (1978).

[26] A. Iniesta and J. García de la Torre, J. Chem. Phys. **92**, 2015 (1990).

[27] R. B. Bird, H. H. Saab, P. J. Dotson, and X. J. Fan, J. Chem. Phys. **79**, 5729 (1983).

[28] S. Wang, J. Chem. Phys. **92**, 7618 (1990).

[29] P. N. Dunlap and L. G. Leal, J. Non-Newtonian Fluid Mech. **23**, 5 (1987).

[30] A. J. Muller, J. A. Odell, and A. Keller, J. Non-Newtonian Fluid Mech. **30**, 99 (1988).

[31] B. H. Zimm, Macromolecules **13**, 592 (1980).

[32] J. Garcia de la Torre, A. Jimenez, and J. J. Freire, Macromolecules **15**, 148 (1982).

[33] J. Garcia de la Torre, M. C. Lopez Martinez, M. M. Tirado, and J. J. Freire, Macromolecules **17**, 2715 (1984).

[34] T. Q. Nguyen and H. H. Kausch, Macromolecules **23**, 5138 (1990).

[35] J. Garcia de la Torre and V. A. Bloomfield, Q. Rev. Biophys. **14**, 81 (1981).

[36] J. Garcia de la Torre, in *Hydrodynamic Properties of Macromolecular Assemblies*, edited by S. Harding and A. Rowe (The Royal Society of Chemistry, London, 1989), pp. 1–41.

[37] J. Garcia de la Torre, M. C. Lopez Martinez, M. M. Tirado, and J. J. Freire, Macromolecules **16**, 1121 (1983).